UNIVERSITY OF KWAZULU-NATAL (HOWARD COLLEGE)

MASTERS THESIS

Discrete Energy Minimisation Optimisation using Graph Cuts for Fluorescence Microscopy

Author:
Ryan NAIDOO

Supervisor:
Dr. Jules-Raymond TAPAMO

A thesis submitted in fulfillment of the requirements for the degree of Master of Science in Engineering

in the

Department of Electrical, Electronic and Computer Engineering
School of Engineering

October 23, 2016

Declaration of Authorship

I, Ryan NAIDOO, declare that this thesis titled, "Discrete Energy Minimisation Optimisation using Graph Cuts for Fluorescence Microscopy" and the work presented in it are my own. I confirm that:

- This work was done wholly or mainly while in candidature for a research degree at this University.
- Where any part of this thesis has previously been submitted for a degree or any other qualification at this University or any other institution, this has been clearly stated.
- Where I have consulted the published work of others, this is always clearly attributed.
- Where I have quoted from the work of others, the source is always given. With the exception of such quotations, this thesis is entirely my own work.
- I have acknowledged all main sources of help.
- Where the thesis is based on work done by myself jointly with others, I have made clear exactly what was done by others and what I have contributed myself.

Signed:

Date:

"Thanks to my solid academic training, today I can write hundreds of words on virtually any topic without possessing a shred of information, which is how I got a good job in journalism."

Dave Barry

UNIVERSITY OF KWAZULU-NATAL (HOWARD COLLEGE)

Abstract

Faculty of Engineering
School of Engineering

Master of Science in Engineering

Discrete Energy Minimisation Optimisation using Graph Cuts for Fluorescence Microscopy

by Ryan NAIDOO

The Thesis Abstract is written here (and usually kept to just this page). The page is kept centered vertically so can expand into the blank space above the title too…

Acknowledgements

The acknowledgments and the people to thank go here, don't forget to include your project advisor…

Contents

List of Figures

List of Tables

List of Algorithms

List of Abbreviations

ACWE	**A**ctive **C**ontours **W**ithout **E**dges
AOD	**A**verage **O**ptical **D**ensity
BCC	**B**oundary **C**hain **C**ode
BFS	**B**readth **F**irst **S**earch
BP	**B**elief **P**ropagation
CCD	**C**harge-**C**oupled **D**evice
CED	**C**oherence **E**nhancing **D**iffusion
CLSM	**C**onfocal **L**aser **S**canning **M**icroscopy
CRF	**C**onditional **R**andom **F**ield
DCC	**D**ifferential **C**hain **C**ode
DFS	**D**epth **F**irst **S**earch
DNA	**D**eoxyribo**n**ucleic **A**cid
DP	**D**ynamic **P**rogramming
DT	**D**elaunay **T**riangulation
EGFP	**E**nhanced **G**reen **F**luorescent **P**rotein
EM	**E**xpectation **M**aximisation
FCS	**F**luorenscence **C**orrelation **S**pectroscopy
FIFO	**F**irst-**I**n **F**irst-**O**ut
FISH	**F**luorenscence **i**n-**s**itu **H**ybridisation
FLIM	**F**luorenscence **L**ifetime **I**maging **M**icroscopy
FRAP	**F**luorenscence **R**ecovery **A**fter **P**hotobleaching
FRET	**F**luorenscence **R**esonance **E**nergy **T**ransfer
GA	**G**enetic **A**lgorithm
GCBLS	**G**raph **C**ut **B**ased **L**evel **S**et
GFP	**G**reen **F**luorescent **P**rotein
GLCM	**G**ray **L**evel **C**o-occurrence **M**atrix
GMM	**G**uassian **M**ixture **M**odelling
GRF	**G**ibbs **R**andom **F**ield
HLF	**H**ighest **L**evel **F**irst
ICC	**I**mmuno**c**yto**c**hemistry
ICF	**I**mmuno**c**yto**f**luorescence
ICM	**I**terated **C**onditional **M**odes
IHC	**I**mmuno**h**isto**c**hemistry
IHF	**I**mmuno**h**isto**f**luorescence
IOD	**I**ntegrated **O**ptical **D**ensity
Laser	**L**ight **A**mplification by **S**timulated **E**mission of **R**adiation
LBP	**L**oopy **B**elief **P**ropagation
LED	**L**ight **E**mitting **D**iode
LoG	**L**aplacian **o**f **G**aussian
MAP	**M**aximum **A** **P**osteriori
MIS	**M**edical **I**mage **S**egmentation

MLP	**M**ulti-**L**ayered **P**erceptron
MRF	**M**arkov **R**andom **F**ield
MST	**M**inimum **S**panning **T**ree
NA	**N**umerical **A**perture
ORI	**O**ptimised **R**otational **I**nvariance
OTF	**O**ptical **T**ransfer **F**unction
PSF	**P**oint **S**pread **F**unction
RF	**R**andom **F**ield
RNA	**R**ibo**n**ucleic **A**cid
SNR	**S**ignal-to-**N**oise **R**atio
TV	**T**otal **V**ariation
UV	**U**ltra**v**iolet

For/Dedicated to/To my…

Chapter 1

Parameter Estimation for ACWE Chan-Vese Segmentation

[Introduction] What is special about the Chan-Vese formulation to the Mumford-Shah evolution energy function. Advantages, disadvantages (parameter estimation). Course of the chapter.

1.1 Graph Cut Model for Chan-Vese Segmentation

Chan-Vese formulation of the Mumford-Shah formulation. Length approximation using discrete representations (cut-metrics). Discrete representation of Chan-Vese formulation. Graph representation and sub-modularity constraint. Insensitivity to initialisation. What do the parameters mean and how do they influence the final result. In this section we briefly reintroduce the graph cut formulation for the Chan-Vese formulation of the Mumford-Shah evolution energy function for image segmentation. The Mumford-Shah model uses gradient descent techniques to obtain a minimum but as previously discussed, **??**, they usually terminate at local minima. By reformulating the energy function in a discrete form that allows for appropriate graph representability, we can use graph cuts, which are able to terminate at a global minimum, to iteratively converge to the optimal solution. For an in-depth exposition into this technique, look to [1–3].

The level set representation of the Mumford-Shah energy function is

$$
\begin{aligned}
F(c_1, c_2, \phi) = \mu \int_\Omega & \delta(\phi(x,y))|\nabla\phi(x,y)|dxdy \\
& + \nu \int_\Omega H(\phi(x,y))dxdy \\
& + \lambda_1 \int_\Omega |u(x,y) - c_1|^2 H(\phi(x,y))dxdy \\
& + \lambda_2 \int_\Omega |u(x,y) - c_2|^2 (1 - H(\phi(x,y)))dxdy,
\end{aligned}
\tag{1.1}
$$

where $u(x,y)$ is the image, $H(\cdot)$ is the Heaviside step function, $\delta(\cdot)$ is the Dirac delta function, $\phi : \Omega \to \Re$ is the level set function, such that:

$$
\begin{aligned}
\omega &= \{(x,y) \in \Omega | \Phi(x_p) > 0\} \text{ Inside the boundary} \\
\bar{\omega} &= \{(x,y) \in \Omega | \Phi(x_p) < 0\} \text{ Outside the boundary} \\
C = \partial\omega &= \{(x,y) \in \Omega | \Phi(x_p) = 0\} \text{ Along the boundary,}
\end{aligned}
\tag{1.2}
$$

c_1 and c_2 are the arithmetic means given by:

$$c_1(\phi) = \frac{\int_\Omega u(x,y)H(\phi(x,y))dxdy}{\int_\Omega H(\phi(x,y))dxdy}, \tag{1.3}$$

$$c_2(\phi) = \frac{\int_\Omega u(x,y)(1-H(\phi(x,y)))dxdy}{\int_\Omega (1-H(\phi(x,y)))dxdy}. \tag{1.4}$$

The piecewise smooth approximation of the image is then

$$u(x,y) = c_1 H(\phi(x,y)) + c_2(1-H(\phi(x,y))). \tag{1.5}$$

Discrete Approximation of Contour Length For the energy function to be represented as a graph, one of the requirements is that it must be in a discrete representation. This means that the length of the contour, the first term in Equation (1.1), must be approximated discretely and be graph representable. This work has already been done by Kolmogorov and Boykov in [4, 5] where they used the Cauchy-Crofton thereom. The thereom states that the length of a curve can be approximated by draw a large number of straight lines from 0 to 2π and counting the number of intersections between the lines and the contour. The mathematical representation is

$$\int_L n_L dL = \int_0^\pi \int_{-\infty}^{\infty} n_L d\rho d\theta = 2\|C\|_E, \tag{1.6}$$

where n_L is the number of intersections between the contour C and the line L, $\|C\|_E$ is the Euclidean length of the contour, $0 < \rho < \infty$ and $0 < \theta < 2\pi$. From this the discrete approximation used by Boykov and Zabih is

$$\|C\|_E = \frac{1}{2}\sum_k n_k \frac{\delta^2 \Delta\theta_k}{|e_k|} = \frac{1}{2}\sum_k n_k w_k \tag{1.7}$$

An example of approximating the contour by two grids is illustrated in Figure 1.1(a) using four families of parallel lines which are 45^{o} apart.

Discrete Representation of Mumford-Shah Function With the exception of the second term in Equation (1.1), the remaining terms are represented easily discretely. For each pixel $p \in \Omega$, let x_p be a binary variable such that

$$x_p = \begin{cases} 0 & \phi(p) \leq 0 \\ 1 & \phi(p) > 0 \end{cases} \tag{1.8}$$

The means can now be calculated using

$$c_1 = \frac{\sum_p u(x,y)x_p}{\sum_p x_p}, \tag{1.9}$$

$$c_2 = \frac{\sum_p u(x,y)(1-x_p)}{\sum_p (1-x_p)}. \tag{1.10}$$

For simplification, $\nu = 0$. To determine contour length using an 8-neighbourhood system, as illustrated in Figure 1.1(b), we set $\Delta\rho = 1$. The weight w_k is assigned to it's corresponding edge e_k. The Euclidean length of the edges is $|e_1| = |e_3| = 1$ and $|e_2| = |e_4| = \sqrt{2}$, therefore

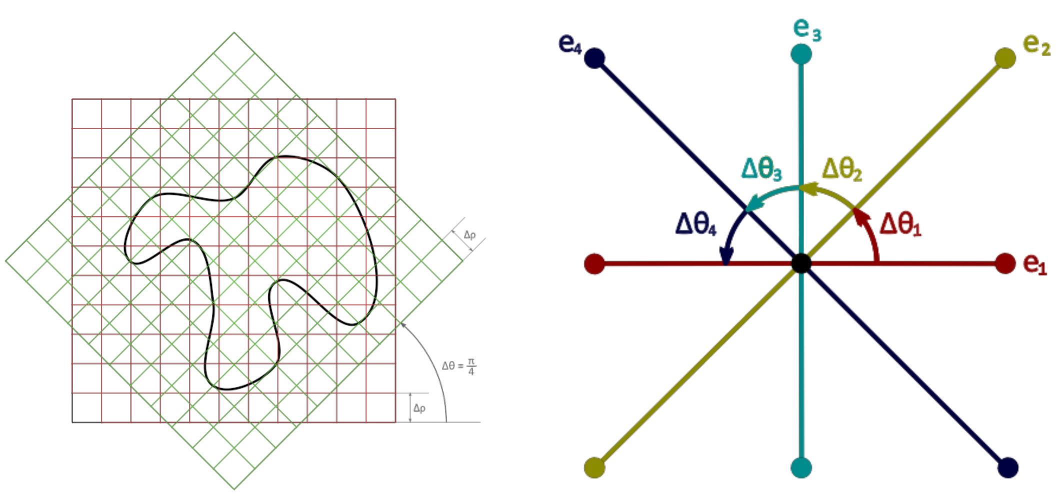

(a) (b)

FIGURE 1.1: **(a)** Cauchy-Crofton length approximation. **(b)** 8-connected neighbourhood system.

the corresponding weights, which are determined using Equation (1.7), is $w_1 = w_3 = \frac{\pi}{8}$ and $w_2 = w_4 = \frac{\pi}{8\sqrt{2}}$. To calculate n_k we need to count the intersections between the lines and the contour. An intersection between two pixels p and q exists *if and only if* x_p and x_q have different labels.

$$n_k = x_p(1 - x_q) + x_q(1 - x_p);\ k = (pq) \in \mathcal{N}_p. \tag{1.11}$$

The contour length can now fully be expressed discretely as

$$\|C\|_E = \sum_{p,q \in e_k} w_k(x_p(1 - x_q) + x_q(1 - x_p)). \tag{1.12}$$

The discrete representation of Equation (1.1) is

$$\begin{aligned} F(x_1, \dots, x_n) = \mu &\sum_{p,q \in e_k} w_k(x_p(1 - x_q) + x_q(1 - x_p)) \\ &+ \lambda_1 \sum_p |u(x,y) - c_1|^2 x_p \\ &+ \lambda_2 \sum_p |u(x,y) - c_2|^2 (1 - x_p) \end{aligned} \tag{1.13}$$

Graph Representation The discrete energy function Equation (1.13) has been shown that it obey the submodularity constraint for graph representability. Therefore the data energy and regularistion energy is

$$E^p(x_p) = \lambda_1 |u(x,y) - c_1|^2 x_p + \lambda_2 |u(x,y) - c_2|^2 (1 - x_p) \tag{1.14}$$

$$E^{pq}(x_p, x_q) = (x_p + x_q - 2x_p x_q) w_{pq} \tag{1.15}$$

The graph for the energy function is constructed as in [6].

1.2 Modified Weighting and Parameter Estimation

What is wrong with the previously described graph weighting. What would we expect from a better weighting system.

1.2.1 Graph Weighting

The first thing we do is normalise the weighting for both the data and smoothing connections. For the weighting of the neighbourhood connections we use the Euclidean distance between adjacent nodes. This results in neigbourhood connections as illustrated in Figure 1.2. The range of pixel intensities is also normlised i.e. $p \in [0, 1]$. The weight of the connection from the source to the node p is given by $E^i(0)|_{i=p} = \lambda_0 |p - c_0|^2$. This is seen as how far away the pixel is from c_0. Similarly, the weight of the connection from the node to the sink is given by $E^i(1)|_{i=p} = \lambda_1 |p - c_1|^2$, i.e. how far way the pixel is from c_1. The fully connected graph for a single node in te 8-connected neighbourhood system is illustrated in Figure 1.2.

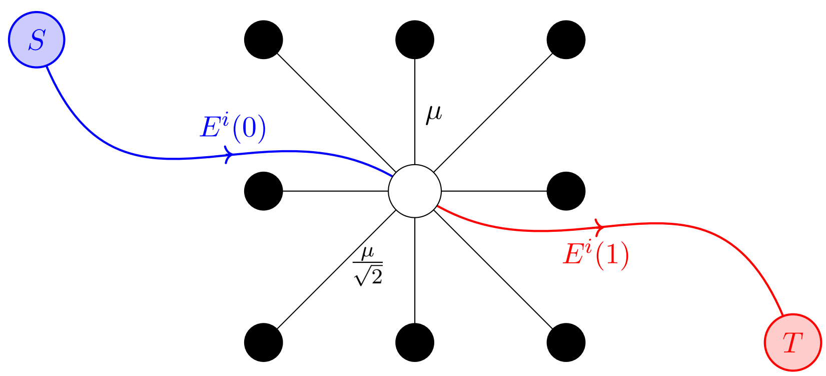

FIGURE 1.2: Fully connected single node.

Describe the modified weighting and parameter relations.

1.2.2 Analysis of Weighting System and Parameter Relationships

Describe the relationship between various parameters including their limits and ranges.

To better understand the relationship between λ_0 and λ_1 and its impact on the final solution we explicitely formalise the dependancy and set

$$\lambda_0 = \alpha \lambda_1. \tag{1.16}$$

Forcing this relation between λ_0 and λ_1 makes further analysis simpler and more intuitive. We can immediately see a constraint on α. Since, we require data connections to be positive, i.e. $E^i(0), E^i(1) \geq 0$ (SEE SECTION??), this gives us a lowerbound on α for positive concavity of the energy functions

$$\alpha > 0 \text{ lowerbound on } \alpha \tag{1.17}$$

We will now analyse the flow through a single node. We use Figure 1.2 to facilitate our explanation. From the neighbourhood connections, in an 8-connected neihgbourhood construction, the maximum flow into or out of a node to its neighbours is

$$f_{max} = 4\mu + 4\frac{\mu}{\sqrt{2}} = \mu\left(2\sqrt{2} + 4\right). \tag{1.18}$$

To guarantee that a node will be place in the set with mean c_0 we know that the incoming flow from the source must completely saturate all flow outlets, this can be expressed as

$$E^i(0) > E^i(1) + \mu\left(2\sqrt{2}+4\right). \tag{1.19}$$

This can be read as *"The source saturates the sink and all neighbourhood connections"*. Similarly to guarantee the node will be in the set with mean c_1

$$E^i(1) > E^i(0) + \mu\left(2\sqrt{2}+4\right). \tag{1.20}$$

This can be read as *"The sink is larger than the source and all neighbourhood connections"*. To aid in understanding the energies we use Figure 1.3.

For quadratic energies with $0 < c_0 < c_1 < 1$, there is a point, between c_0 and c_1, where the incoming flow from the source is completely saturates the sink with no excess remaining. This point, where the energies are equal, we call p_e, i.e. $E_0(p_e) = E_1(p_e)$. This point of zero net flow can be found as follows

$$\begin{aligned}
E^{i=p_e}(1) &= E^{i=p_e}(0)\\
\lambda_1(p_e - c_1)^2 &= \lambda_0(p_e - c_0)^2\\
\frac{(p_e - c_0)^2}{(p_e - c_1)^2} &= \frac{\lambda_1}{\lambda_0}\\
\frac{p_e - c_0}{p_e - c_1} = \sqrt{\frac{\lambda_1}{\lambda_0}} \quad &\text{or} \quad \frac{p_e - c_0}{p_e - c_1} = -\sqrt{\frac{\lambda_1}{\lambda_0}}
\end{aligned}$$

We know that

$$\begin{aligned}
&c_0 < p_e < c_1\\
\therefore\, p_e - c_0 > 0 \quad &\text{and} \quad p_e - c_1 < 0
\end{aligned}$$

It follows, directly , that

$$\begin{aligned}
\frac{p_e - c_1}{p_e - c_0} &= -\sqrt{\frac{\lambda_1}{\lambda_0}}\\
\frac{(p_e - c_0) + (c_0 - c_1)}{p_e - c_0} &= -\sqrt{\frac{\lambda_1}{\lambda_0}}\\
\frac{c_0 - c_1}{p_e - c_0} &= -\left(\sqrt{\frac{\lambda_1}{\lambda_0}} + 1\right)\\
p_e = c_0 + \frac{c_1 - c_0}{\sqrt{\frac{\lambda_1}{\lambda_0}} + 1}
\end{aligned}$$

After substituting the relation in Equation (1.16) we get

$$p_e = c_0 + \frac{c_1 - c_0}{\sqrt{\alpha} + 1} \tag{1.21}$$

The point where the energies are equal, p_e, is shown in Figure 1.3.

Analysis of the relationship between p_e and α From Equation (1.21) we note that there is one

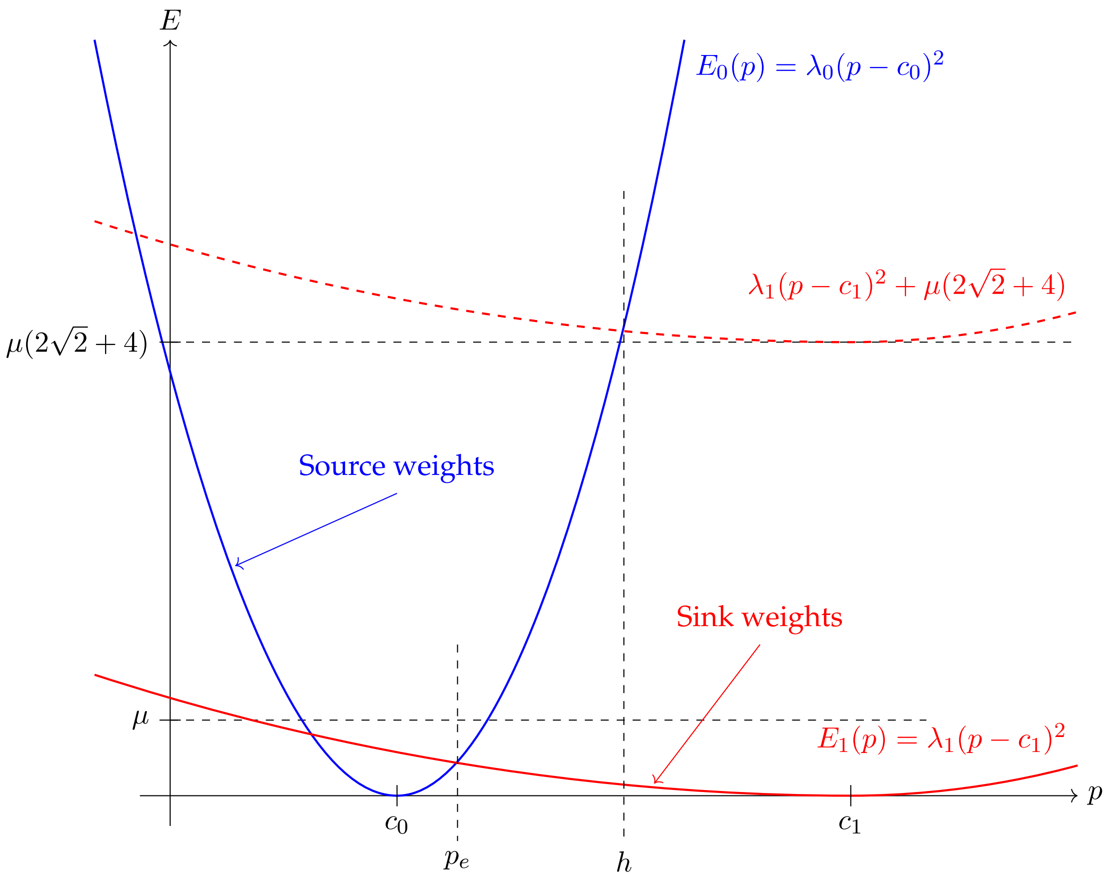

FIGURE 1.3: Data energy functions plot.

tunable parameter, i.e. α. We can see that p_e and α are inversely related. This is expressed mathematically as

$$\text{if } \alpha = 1, p_e = c_0 + \frac{c_1 - c_0}{1 + \sqrt{1}} = \frac{c_0 + c_1}{2} \qquad \text{(midpoint between } c_0 \text{ and } c_1\text{)}$$

$$\lim_{\alpha \to \infty} p_e = \lim_{\alpha \to \infty} c_0 + \frac{c_1 - c_0}{1 + \sqrt{1}} = c_0 \qquad \text{(maximum } \alpha \text{ yields lowerbound on } p_e\text{)}$$

$$\lim_{\alpha \to 0} p_e = \lim_{\alpha \to 0} c_0 + \frac{c_1 - c_0}{1 + \sqrt{0}} = c_1 \qquad \text{(minimum } \alpha \text{ yields upperbound on } p_e\text{)}$$

The relationship between p_e and α is illustrated in Figure 1.4.

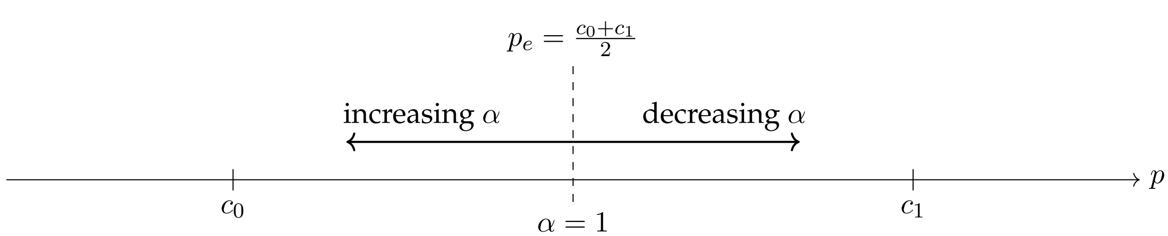

FIGURE 1.4: Relationship between α and p_e.

Figuring α If we are able to make good estimates on p_e, c_0 and c_1 for the final segmented image, then it is possible to calculate α as follows:

$$\begin{aligned} p_e &= c_0 + \frac{c_1 - c_0}{\sqrt{\alpha} + 1} \\ 1 + \sqrt{\alpha} &= \frac{c_1 - c_0}{p_e - c_0} \\ \alpha &= \left(\frac{c_1 - c_0}{p_e - c_0} - 1 \right)^2 \end{aligned} \tag{1.22}$$

Lowerbound on μ When we found the point, p_e, where the energies are equal in Equation (1.21), we ignored the other solution as it was not within the range from c_0 to c_1. Let this point be p_{e^*}. If this point is positive and $0 < p_{e^*} < c_0$ then we must ensure that at no point within this range that the source flow saturates all the outgoing edges. This force a limit on how low μ can be. This is only of significant concern when $\alpha > 1$. We only need to concern ourselve with the point $p = 0$ as this is the point where the difference $E^i(0) - E^i(1)$ is the largest. The lowerbound on μ can be obtained as follows

$$\begin{aligned} E^i(0)|_{p_i=0} &< E^i(1)|_{p_i=0} + \mu\left(2\sqrt{2} + 4\right) \\ \lambda_0 c_0^2 &< \lambda_1 c_1^2 + \mu\left(2\sqrt{2} + 4\right) \\ \therefore \mu\left(2\sqrt{2} + 4\right) &> \lambda_0 c_0^2 - \lambda_1 c_1^2 \\ \mu &> \frac{\lambda_0 c_0^2 - \lambda_1 c_1^2}{\left(2\sqrt{2} + 4\right)} \end{aligned}$$

Taking into account the relation in Equation (1.16) this becomes

$$\mu > \frac{\lambda_1(\alpha c_0^2 - c_1^2)}{\left(2\sqrt{2} + 4\right)} \tag{1.23}$$

Absolutely in the source set From Equation (1.19) we can see that there is a point beyond which all nodes which correspond to pixel value higher than that point will be saturated and have excess flow which means that they will be in the source set. We will call this point the *saturation point* and denote it by h. This is shown in Figure 1.3. This point can be determined as follows:

$$\begin{aligned} \lambda_0(h - c_0)^2 &> \lambda_1(h - c_1)^2 + f_{max} \\ \lambda_0(h - c_0)^2 - \lambda_1(h - c_1)^2 &> f_{max} \\ (\lambda_0 - \lambda_1)h^2 + (-2\lambda_0 c_0 + 2\lambda_1 c_1)h + (\lambda_0 c_0^2 - \lambda_1 c_1^2 - f_{max}) &> 0 \end{aligned}$$

The solutions to h are

$$h = \frac{(2\lambda_0 c_0 - 2\lambda_1 c_1) \pm \sqrt{(-2\lambda_0 c_0 + 2\lambda_1 c_1)^2 - 4(\lambda_0 - \lambda_1)(\lambda_0 c_0^2 - \lambda_1 c_1^2 - f_{max})}}{2(\lambda_0 - \lambda_1)}$$

Substituting the relation in Equation (1.16)

$$
\begin{aligned}
h &= \frac{(\alpha c_0 - c_1) \pm \sqrt{(c_1 - \alpha c_0)^2 - (\alpha - 1)(\alpha c_0^2 - c_1^2 - \frac{f_{max}}{\lambda_1})}}{\alpha - 1} \\
&= \frac{(\alpha c_0 - c_1) \pm \sqrt{\alpha (c_0 - c_1)^2 + \frac{f_{max}}{\lambda_1}(\alpha - 1)}}{\alpha - 1}
\end{aligned}
$$

If the μ is greater than the lowerbound in Equation (1.23) then there is only one solution to h which is of importance. This is the positive solution for h which is

$$
h = \frac{(\alpha c_0 - c_1) + \sqrt{\alpha (c_0 - c_1)^2 + \frac{\mu(2\sqrt{2}+4)}{\lambda_1}(\alpha - 1)}}{\alpha - 1} \tag{1.24}
$$

This point is marked off in Figure 1.3.

Determining λ_1 Given good approximations for c_0, c_1, α, h and μ, we can calculate the appropriate value for λ_1. We proceed from Equation (1.19) as follows

$$
\begin{aligned}
\lambda_0 (h - c_0)^2 &= \lambda_1 (h - c_1)^2 + \mu(2\sqrt{2} + 4) \\
\lambda_1 (\alpha (h - c_0)^2 - (h - c_1)^2) &= \mu(2\sqrt{2} + 4)
\end{aligned}
$$

$$
\lambda_1 = \frac{\mu(2\sqrt{2} + 4)}{\alpha (h - c_0)^2 - (h - c_1)^2} \tag{1.25}
$$

The parameter estimation is based on the assumption that sufficiently good approximations for c_0, c_1, p_e and h can be obtained. From these approximation we calculate the approximation for α using Equation (1.22). The parameters μ and α are related and aren't seperable, therefore we set choose to set μ. We can then calculate λ_1 using Equation (1.25). For the chosen μ we can calculate the upperbound on α to ensure that the constraint Equation (1.23) is met. The constraint on λ_1 is calculated as follows

$$
\mu \left(2\sqrt{2} + 4\right) > \lambda_1 (\alpha c_0^2 - c_1^2)
$$

$$
\lambda_1 < \frac{\mu \left(2\sqrt{2} + 4\right)}{\alpha c_0^2 - c_1^2} \tag{1.26}
$$

Finally λ_0 can be calculated using Equation (1.16).

1.2.3 Tuning Parameters for Fluorescence Microscopy

What sort of image properties are we tuning for? E.g. dark bg, low contrast, etc. Parameters limits and ranges.

1.3 Experimental Results

Present and analyse the experimental results.

Appendix A

Introduction to Graph Theory

Graph A graph G is a pair (V, E), where V is the set of nodes/vertices and E is the set of edges consisting of pairs (u, v) where $u, v \in V$. The graph is assumed to be finite i.e. $|V| = n$ and $|E| = m$.

In an **undirected graph**, the edge (u, v) and (v, u) are not distinct. That is, they refer to the same edge. However, in a **directed graph**, the two edge are now distinct. In a directed graph with edge (u, v), u is known as the **tail** and v is know as the **head**. In directed graphs, edges, also known as arcs, are depicted by placing arrowheads at the head of the edge. Given an edge $e = (u, v)$, u and v are said to be **incident** on e. A graph is said to be **simple** if it does not contain any self-loops. A **self-loop** is an edge with of its end points being the same vertex.

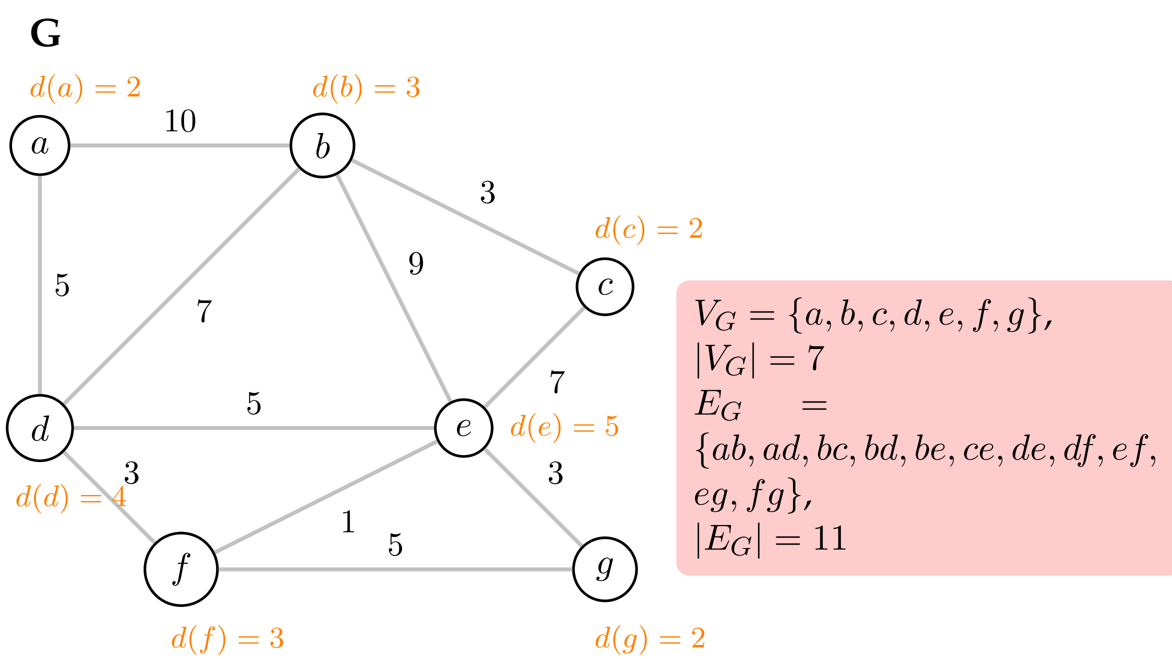

FIGURE A.1: Undirected weighted graph **G**. The degree of each node is shown next to the corresponding node. The graph is simple. The red box shows the vertex set, V_G, and edge set, E_G, and their corresponding norm.

Degree The degree of a vertex v is the number of edges incident on it. $deg(v) = |\{(u, v), (v, u) \in E\}|$. A self-loop counts for 2.

If a graph is directed, also known as a **digraph**, then a node v has an **in-degree** $d_{in}(v)$ and an **out-degree** $d_{out}(v)$. A digraph is said to be **balanced** if $d_{in}(v) = d_{out}(v), \forall v \in V$.

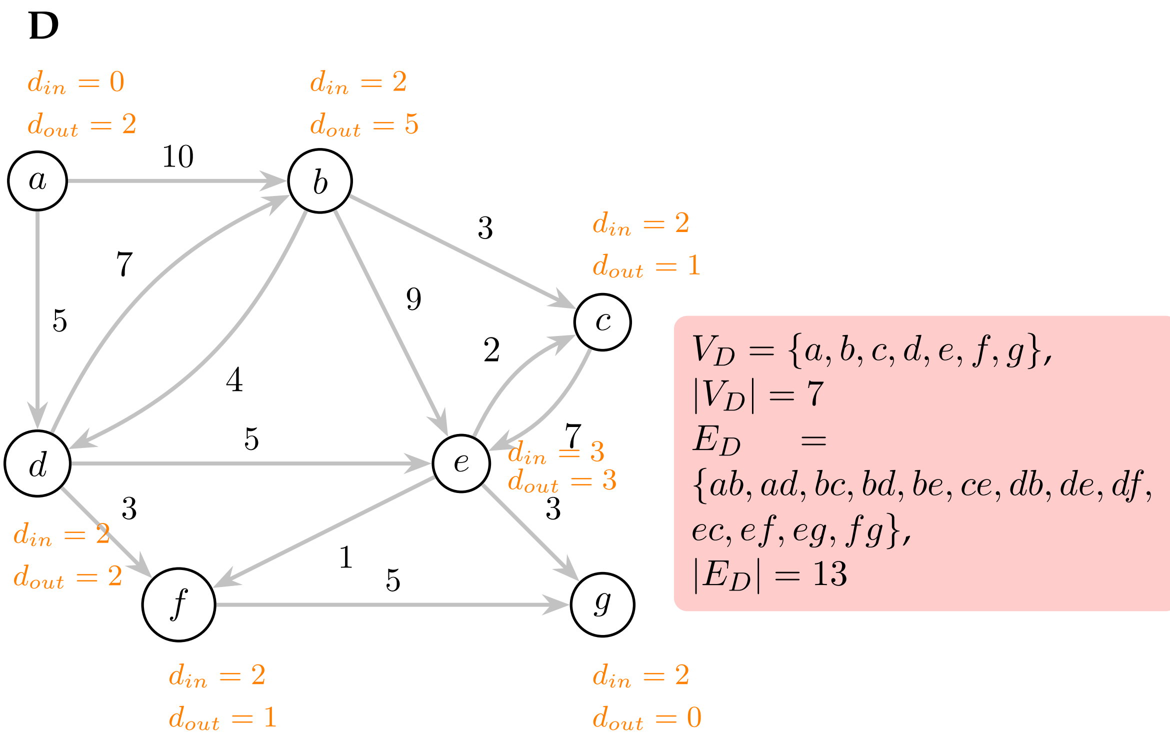

FIGURE A.2: Directed weighted graph (Digraph) **D**. The in-degree and out-degree is shown next to each node. The graph is simple and not balanced. The red box shows the vertex set, V_D, and edge set, E_D, and their corresponding norm.

Subgraph A graph $G' = (V', E')$ is said to be a sub-graph of $G = (V, E)$, denoted as $G' \subseteq G$, if $V' \subseteq V$ and $E' \subseteq E$.

Clique A clique is a maximal subgraph.

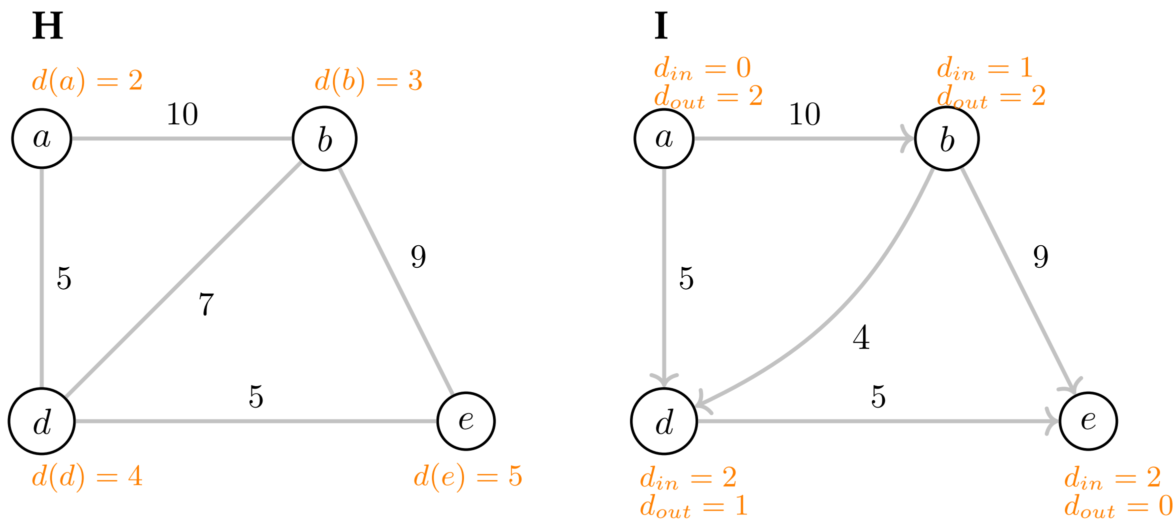

$V_H = \{a, b, d, e\} \subseteq V_G$,
$|V_H| = 4$
$E_H = \{ab, ad, bd, be, de\} \subseteq E_G$,
$|E_H| = 5$

$V_I = \{a, b, d, e\} \subseteq V_D$,
$|V_I| = 4$
$E_I = \{ab, ad, bd, be, de\} \subseteq E_D$,
$|E_I| = 5$

FIGURE A.3: Undirected weighted graph **H** is a subgraph of **G** in Figure XX, **H** $\subseteq$ **G**. Directed weighted graph **I** is a subgraph of **D** in Figure XX, **I** $\subseteq$ **D**. The degree of each node is shown next to the corresponding node. The red box shows the vertex set, the edge set and their corresponding norms.

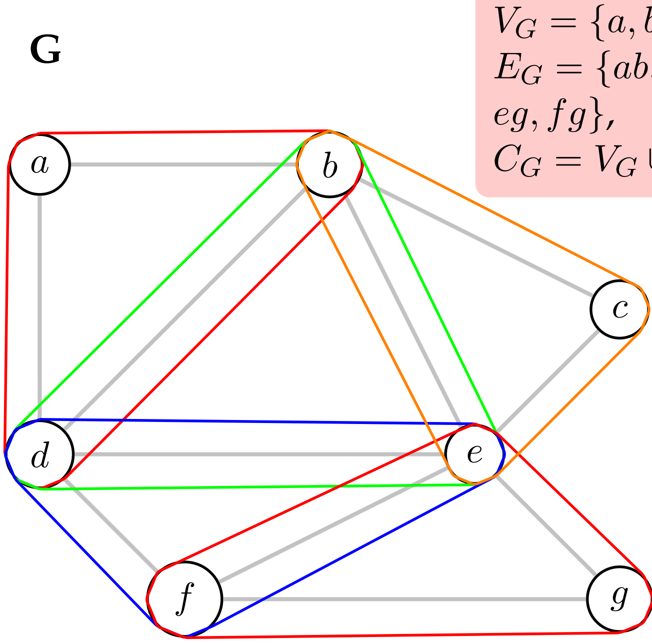

$V_G = \{a, b, c, d, e, f, g\}$,
$E_G = \{ab, ad, bc, bd, be, ce, de, df, ef, eg, fg\}$,
$C_G = V_G \cup E_G \cup \{abd, bce, efg, edf, bde\}$

FIGURE A.4: Cliques of the undirected weighted graph **G**. The maximal cliques are shown by the hyperedges that encompass the nodes of that clique.

Appendix B

Cell Images Dataset

The dataset is composed of two subsets. One as the sample set and one as the test set. The sample set is used for tuning parameters and testing theories or predictions. This dataset is composed of images that are relatively simple but still try to maintain some of the variation of images obtained in fluorescence microscopy. The other dataset is the test set. This dataset is contains more complex images and is used to test the robustness of the segmentation schemes or techniques. We aim for a larger coverage of the types of images that are frequently obtained in fluorescence microscopy.

B.1 Sample Set

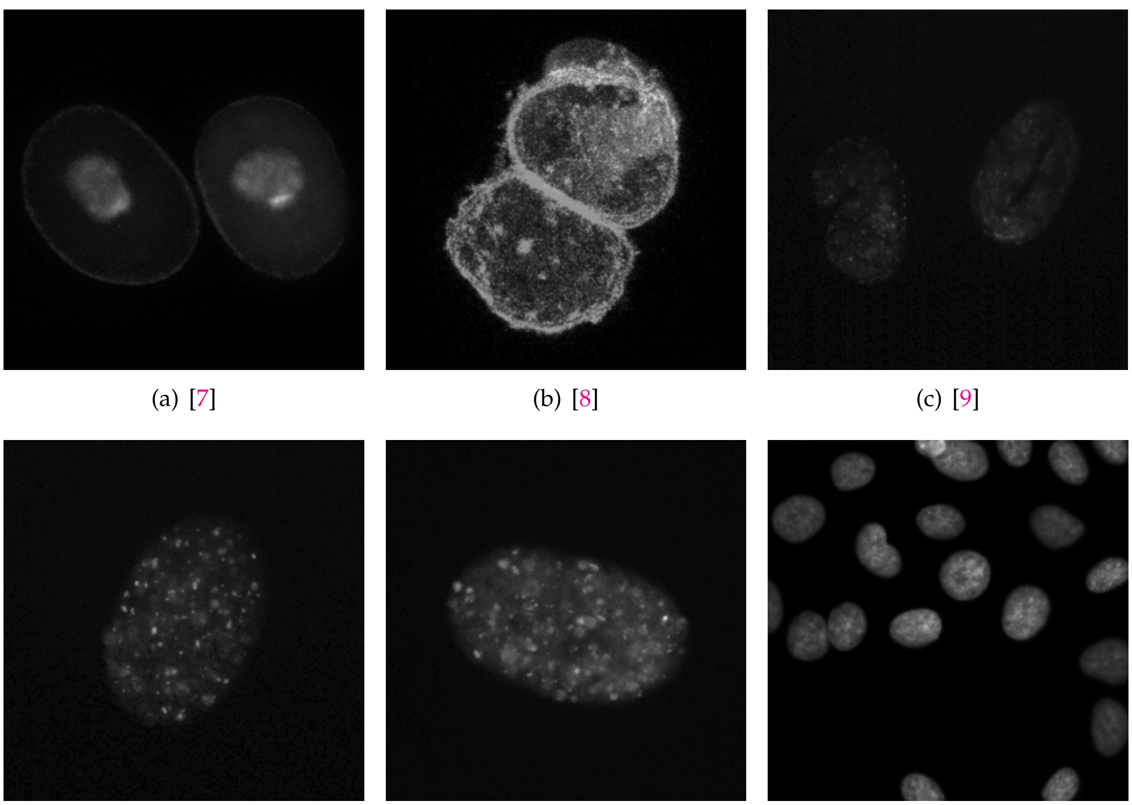

(a) [7] (b) [8] (c) [9]

(d) [10] (e) [11] (f)

FIGURE B.1: Sample set.

B.2 Test Set

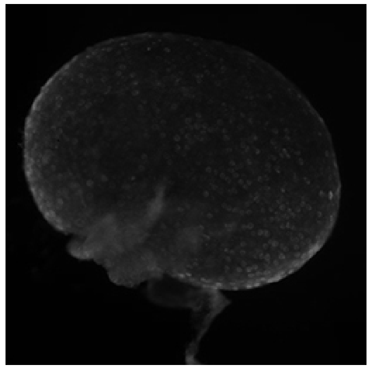

(a) [12]

FIGURE B.2: Uneven Illumination

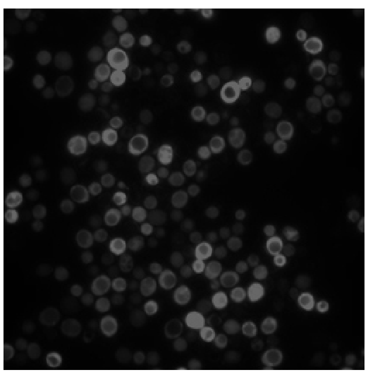

(a) [13]

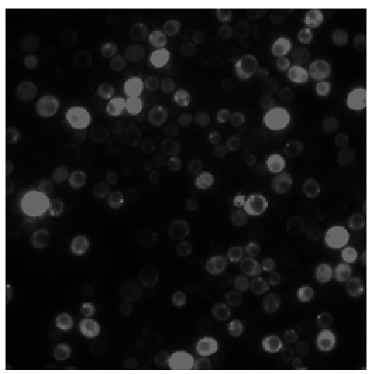

(b) [14]

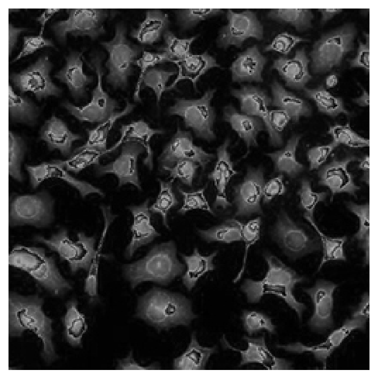

(c) [15]

FIGURE B.3: High cell density

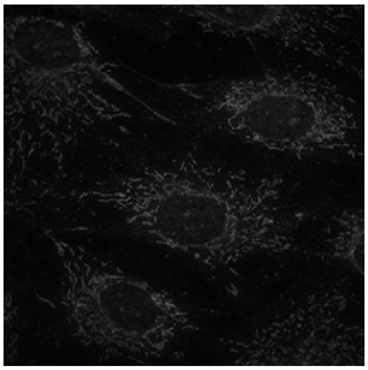

(a) [16]

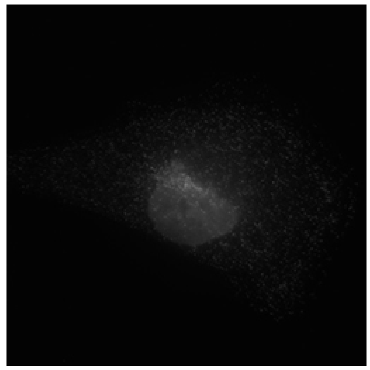

(b) [17]

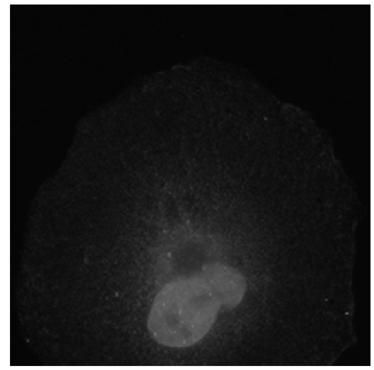

(c) [18]

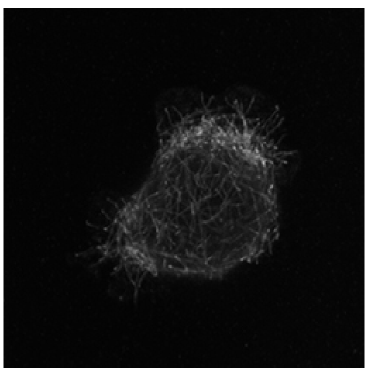

(d) [19]

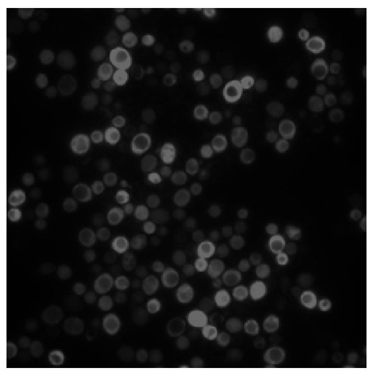

(e) [13]

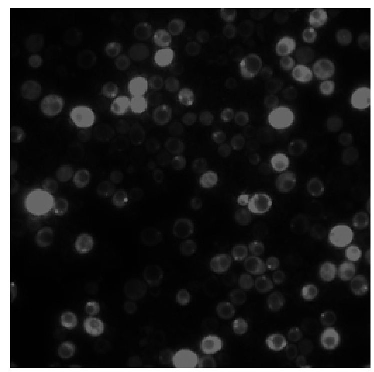

(f) [14]

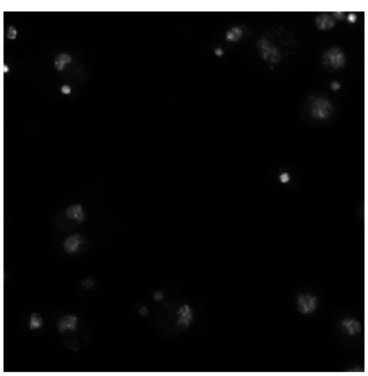

(g) [20]

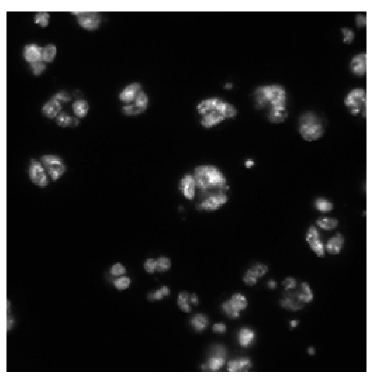

(h) [21]

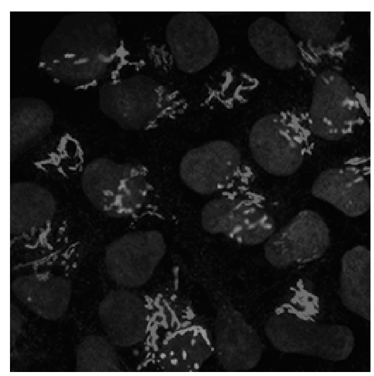

(i) [22]

FIGURE B.4: Multi-modal (non-bi-modal)

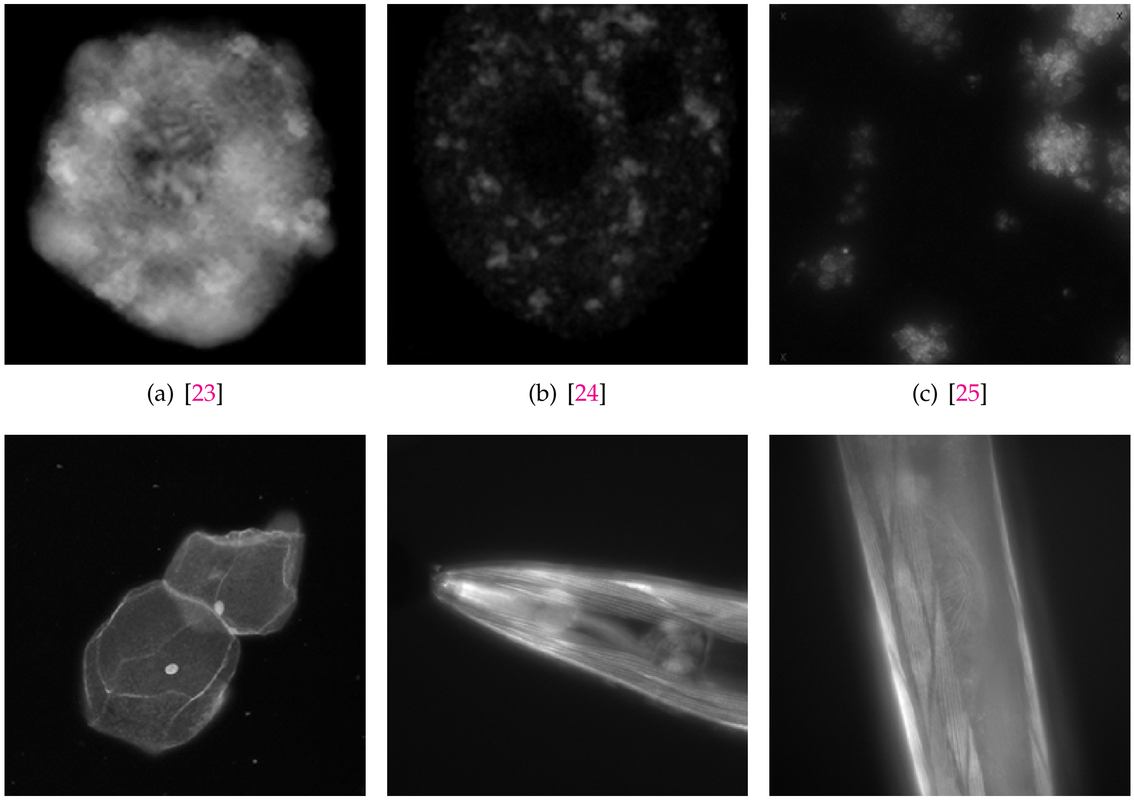

(a) [23] (b) [24] (c) [25]

(d) [26] (e) [27] (f) [28]

FIGURE B.5: Hazy/Glowing Edges

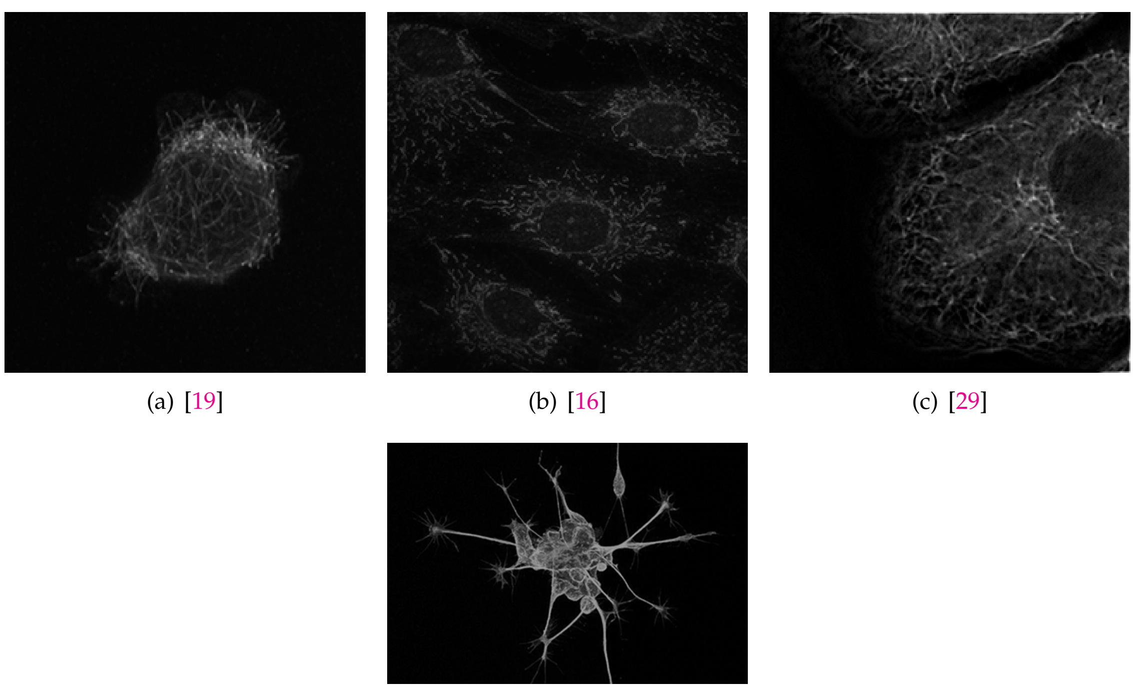

(a) [19] (b) [16] (c) [29]

(d) [30]

FIGURE B.6: Thin Tentacles

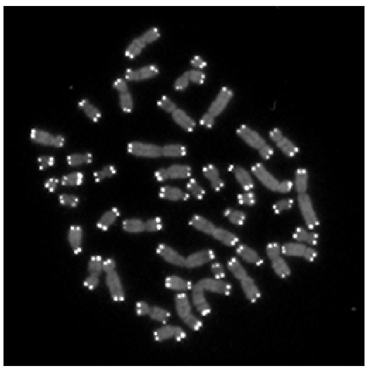

(a) [31]

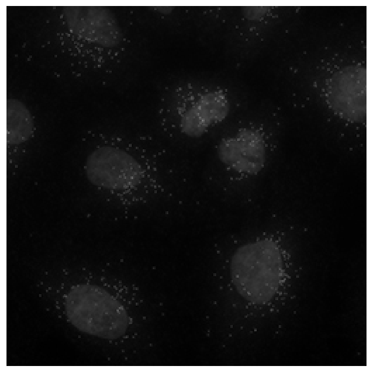

(b) [32]

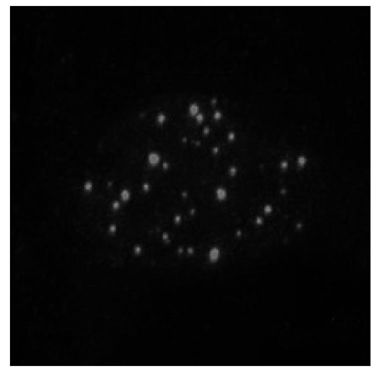

(c) [33]

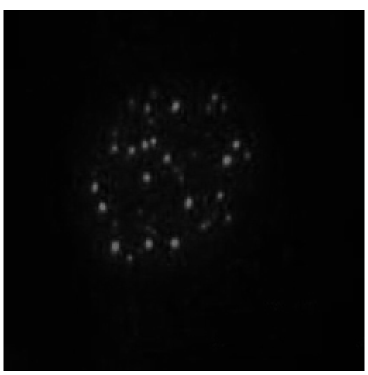

(d) [34]

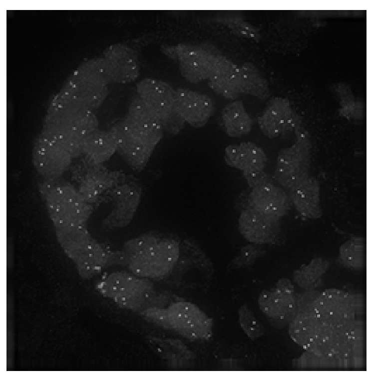

(e) [35]

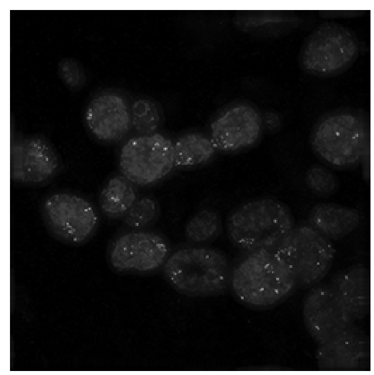

(f) [36]

FIGURE B.7: Bright Spots and Speckles

Bibliography

[1] David Mumford. "Optimal approximation by piecewise smooth functions and associated variational problems". In: *Commun. Pure Applied Mathematics* (1989), pp. 577–685.

[2] T. F. Chan and L. A. Vese. "Active Contours Without Edges". In: *Trans. Img. Proc.* 10.2 (2001), pp. 266–277. ISSN: 1057-7149. DOI: 10.1109/83.902291. URL: http://dx.doi.org/10.1109/83.902291.

[3] Noha El Zehiry et al. "Graph Cut Optimization for the Mumford-Shah Model". In: *The Seventh IASTED International Conference on Visualization, Imaging and Image Processing*. VIIP '07. Palma de Mallorca, Spain: ACTA Press, 2007, pp. 182–187. ISBN: 978-0-88986-692-8. URL: http://dl.acm.org/citation.cfm?id=1659167.1659203.

[4] Vladimir Kolmogorov and Yuri Boykov. "What Metrics Can Be Approximated by Geo-Cuts, Or Global Optimization of Length/Area and Flux." In: *ICCV*. IEEE Computer Society, 2005, pp. 564–571. ISBN: 0-7695-2334-X. URL: http://dblp.uni-trier.de/db/conf/iccv/iccv2005-1.html#KolmogorovB05.

[5] Yuri Boykov. "Computing geodesics and minimal surfaces via graph cuts". In: *in International Conference on Computer Vision*. 2003, pp. 26–33.

[6] Vladimir Kolmogorov and Ramin Zabih. "What energy functions can be minimized via graph cuts?" In: *IEEE Transactions on Pattern Analysis and Machine Intelligence* 26.2 (2004), pp. 65–81.

[7] S. Huang et al. *CIL 9233*. Picture. (accessed July 6, 2015). URL: http://www.cellimagelibrary.org/images/9233.

[8] R. Mejia. *CIL 11996*. Picture. http://www.cellimagelibrary.org/images/11996. (accessed July 6, 2015).

[9] E. Morselli. *CIL 13902*. Picture. http://www.cellimagelibrary.org/images/13902. (accessed July 6, 2015).

[10] E. Morselli. *CIL 13903*. Picture. http://www.cellimagelibrary.org/images/13903. (accessed July 6, 2015).

[11] E. Morselli. *CIL 13904*. Picture. http://www.cellimagelibrary.org/images/13904. (accessed July 6, 2015).

[12] Prue Talbot. *CIL 12627*. Picture. (accessed October 21, 2016). URL: http://www.cellimagelibrary.org/images/12627.

[13] Eugenia Morselli et al. *CIL 13899*. Picture. (accessed October 21, 2016). URL: http://www.cellimagelibrary.org/images/13899.

[14] Eugenia Morselli et al. *CIL 13901*. Picture. (accessed October 21, 2016). URL: http://www.cellimagelibrary.org/images/13901.

[15] Weimiao Yu et al. *CIL 40217*. Picture. (accessed October 21, 2016). URL: http://www.cellimagelibrary.org/images/40217.

[16] Linda Parysek. *CIL 195*. Picture. (accessed October 21, 2016). URL: http://www.cellimagelibrary.org/images/195.

[17] Allen Liu and Sandra L. Schmid. *CIL 10102*. Picture. (accessed October 21, 2016). URL: http://www.cellimagelibrary.org/images/10102.

[18] Allen Liu and Sandra L. Schmid. *CIL 10104*. Picture. (accessed October 21, 2016). URL: http://www.cellimagelibrary.org/images/10104.

[19] Azusa Hotta et al. *CIL 12294*. Picture. (accessed October 21, 2016). URL: http://www.cellimagelibrary.org/images/12294.

[20] Anne Carpenter. *CIL 21749*. Picture. (accessed October 21, 2016). URL: http://www.cellimagelibrary.org/images/21749.

[21] Anne Carpenter. *CIL 21759*. Picture. (accessed October 21, 2016). URL: http://www.cellimagelibrary.org/images/21759.

[22] M. Deshmukh et al. *CIL 41066*. Picture. (accessed October 21, 2016). URL: http://www.cellimagelibrary.org/images/41066.

[23] Olga Pontes and Craig Pikaard. *CIL 188*. Picture. (accessed October 21, 2016). URL: http://www.cellimagelibrary.org/images/188.

[24] R.I. Kumaran, Z. Lazar, and David L. Spector. *CIL 10093*. Picture. (accessed October 21, 2016). URL: http://www.cellimagelibrary.org/images/10093.

[25] Anne Carpenter. *CIL 32140*. Picture. (accessed October 21, 2016). URL: http://www.cellimagelibrary.org/images/32140.

[26] Arjan Tibbe. *CIL 40968*. Picture. (accessed September 9, 2016). URL: http://www.cellimagelibrary.org/images/40968.

[27] Nikita Orlov, Wendy Iser, and Cathy Wolkow. *CIL 1057*. Picture. (accessed October 21, 2016). URL: http://www.cellimagelibrary.org/images/1057.

[28] Nikita Orlov, Wendy Iser, and Cathy Wolkow. *CIL 1265*. Picture. (accessed October 21, 2016). URL: http://www.cellimagelibrary.org/images/1265.

[29] Michael Cammer and Phyllis Novikoff. *CIL 35278*. Picture. (accessed October 21, 2016). URL: http://www.cellimagelibrary.org/images/35278.

[30] Kate Nobes and Mark Shipman. *CIL 38974*. Picture. (accessed October 21, 2016). URL: http://www.cellimagelibrary.org/images/38974.

[31] Hesed Padilla-Nash and Thomas Ried. *CIL 228*. Picture. (accessed October 21, 2016). URL: http://www.cellimagelibrary.org/images/228.

[32] Jr. Arturo Orjalo, Sally Coassin, and Hans Johansson. *CIL 41066*. Picture. (accessed October 21, 2016). URL: http://www.cellimagelibrary.org/images/41066.

[33] Yi-Chun Maria Chen. *CIL 37338*. Picture. (accessed October 21, 2016). URL: http://www.cellimagelibrary.org/images/37338.

[34] Yi-Chun Maria Chen. *CIL 37339*. Picture. (accessed October 21, 2016). URL: http://www.cellimagelibrary.org/images/37339.

[35] Karen Meaburrn et al. *CIL 13432*. Picture. (accessed October 21, 2016). URL: http://www.cellimagelibrary.org/images/13432.

[36] Karen Meaburrn et al. *CIL 13438*. Picture. (accessed October 21, 2016). URL: http://www.cellimagelibrary.org/images/13438.